

Characteristics of TiO₂ Compact Layer prepared for DSSC application

Nicholas Musila¹, Mathew Munji¹, Justus Simiyu², Eric Masika¹, Raphael Nyenge¹,
Miriam Kineene¹

¹ *Kenyatta University*

P. O. Box 43844-00100, Nairobi, Kenya

² *University of Nairobi*

P. O. Box 30197-00100, Nairobi, Kenya

DOI: [10.22178/pos.39-6](https://doi.org/10.22178/pos.39-6)

LCC Subject Category:

[TP155-156](#)

Received 16.09.2018

Accepted 24.10.2018

Published online 31.10.2018

Corresponding Author:

Nicholas Musila

musilanicholas@gmail.com

© 2018 The Authors. This article is licensed under a [Creative Commons Attribution 4.0 License](#) 

Abstract. Dye-sensitized solar cells (DSSCs) offer an economically reliable and suitable alternative in moderating the challenges presented by the existing convectional photovoltaic cells. However, the efficiency of dye-sensitized solar cells has remained relatively low. For this reason, this research was aimed at studying the characteristics of TiO₂ compact layer that can be applied in DSSCs as a way of improving efficiency. To achieve this, TiO₂ compact layer was deposited on a conductive glass substrate by using Holmarc's Spray Pyrolysis system, using Ultrasonic Spray Head and spraying in the vertical geometry. X-ray Diffraction studies revealed that TiO₂ compact layer was of anatase phase and had tetragonal crystalline structure. Raman spectroscopy showed that the most intense peak appeared at 142 cm⁻¹ due to the external vibration of the anatase structure. Hall Effect studies revealed that TiO₂ compact layer has a high density of charge carriers' value of 1.25 × 10¹⁹ cm⁻³ hence it can be used in DSSC applications.

Keywords: Raman spectroscopy; compact layer; dye sensitized solar cell; morphology index; tetragonal crystalline structure; specific surface area; spray pyrolysis.

INTRODUCTION

Dye-sensitized nano-structured solar cells (DSSCs) present themselves as a viable alternative to fossil fuels and silicon-based solar cell technology in meeting the current state of energy demand [1]. They have a central role to play in providing renewable energy. The development of these solar cells generates not only a source of electricity but thermal energy as well from solar energy [2].

However, since DSSCs fabricated from TiO₂ films were discovered, they have had low efficiencies compared to the other commercial solar cells [3]. Among other causes of low efficiency, the structure of the photo-anode electrode is one of the main sources. The nature of the coating on the photo-anode directly contributes on the solar cell performance due to the light harvesting capability, among other factors [4].

Since conversion efficiency of any solar cell is key to commercial competition in the market, there is

need to study characteristics of TiO₂ compact layer, which can be introduced in between the photo-anode electrode and the hole-transport material, as a method of improving the performance of the solar cell [5]. In this study, the electrical, morphological and structural characteristics of TiO₂ compact layer were studied.

EXPERIMENTAL PROCEDURE

The TiO₂ compact layer was deposited onto FTO glass substrates by Holmarc's Spray Pyrolysis system, using Ultrasonic Spray Head, spraying in the vertical geometry. The nozzle used ultrasonic atomization and was operated at a frequency of 40 kHz and its scan speed was 25 mm/s. The nozzle to substrate distance was kept constant at 15 cm, the substrate temperature was maintained at 450 °C and the deposition time was set at 1 minute. Pressurized air (at 6 bar) was used as shaping gas and the solution was sprayed with a rate of 2 ml/min.

The crystalline structure of TiO₂ compact layer was investigated by X-ray diffraction, using a Bruker AXS D8 ADVANCE (Bruker Corporation of Germany). X-ray diffractometer was operated in a Bragg-Brentano configuration (Cu-K α X-rays of wavelength (λ) = 1.5406 Å). XRD pattern of TiO₂ compact layer was obtained for 2(θ) angle between 10° and 80°. In order to quantify the particle size, the mean crystallite size (D) was estimated by applying the Scherrer equation to the strongest plane diffraction peak. D-spacing, specific surface area, morphology index, and dislocation density analyses were done from the XRD pattern obtained.

Confocal Raman microscope and spectrometer was used in Raman spectroscopy analysis of TiO₂ compact layer. 514 nm wavelength argon ion laser was used in the excitation of the TiO₂ compact layer. The analysis of the scattered light was done by a Jobin Yvon U1000 double monochromator while the Raman signal detection was done by a photomultiplier tube (PMT) whose resolution was less than 1 cm⁻¹.

Digital flux/Gauss meter was used in the Hall Effect measurement where the Hall voltage (V_H) and current (I) values of TiO₂ compact layer were recorded upon the application of the magnetic field. The samples to be studied were mounted individually onto a printed circuit, clamped and attached to a stand placed between electromagnetic poles. The Hall voltage was measured in the z-axis direction, the current in the x-axis and the magnetic field in the y-axis direction. The Hall coefficient (R_H), the density of charge carriers (n_H) and Hall mobility (μ_H) of the TiO₂ compact layer were calculated.

The samples were then mounted on a holder inserted in the scanning electron microscope (Carl Zeiss Sigma VP FE-SEM). Coating using a slim layer of 20 nm to 30 nm of platinum was done to increase the conductivity and to prevent the build-up of high voltage charges of the thin films in the scanning electron microscope. The voltage was set at 2 kV and the working distance was set at 2.0 mm.

RESULTS AND DISCUSSION

XRD analysis of TiO₂ compact layer

Figure 1 shows the measured and fitted XRD spectra of TiO₂ compact layer. From the figure, there were seven XRD peaks. The first TiO₂ peak was obtained at 25.83° at plane orientation (101). The most pronounced peak was found at

38.24° at plane orientation (103). These two major peaks confirmed that the prepared TiO₂ compact layer had a pure anatase phase [6].

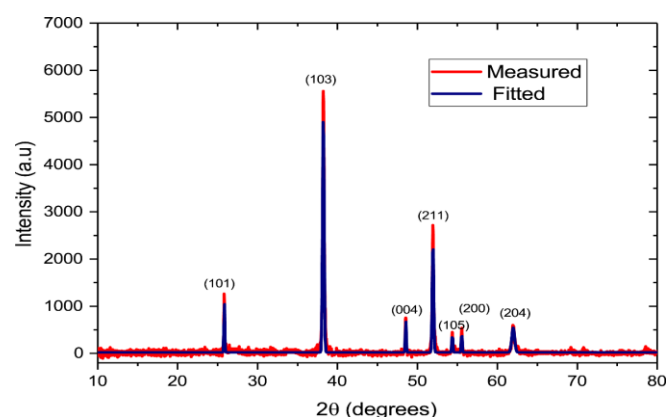


Figure 1 – XRD spectra of TiO₂ compact layer for both measured and fitted data

There were other five peaks at 2 θ angle values of 48.53°, 51.94°, 54.37°, 55.54° and 61.99° respectively. These peaks were at plane orientations (004), (211), (105), (200) and (204) respectively which agreed well with Crystallography Open Database (COD) card number 96-152-6932 [7].

Particle size and the d-spacing of the TiO₂ compact layer. As it is seen from Figure 1, the major XRD peaks had large intensity values which showed that the compact layer had tetragonal crystalline structure which had cell parameters $a = 3.7710$ Å and $c = 9.4300$ Å [7]. In addition, these peaks have broad diffraction which indicates small crystallite size [8]. The particle size of the peak with the highest intensity was 38.17 nm while the spacing between planes was found to be 2.3508 nm.

Figure 2 shows the diffraction broadening of the TiO₂ film at 2 θ angle of 51.94°.

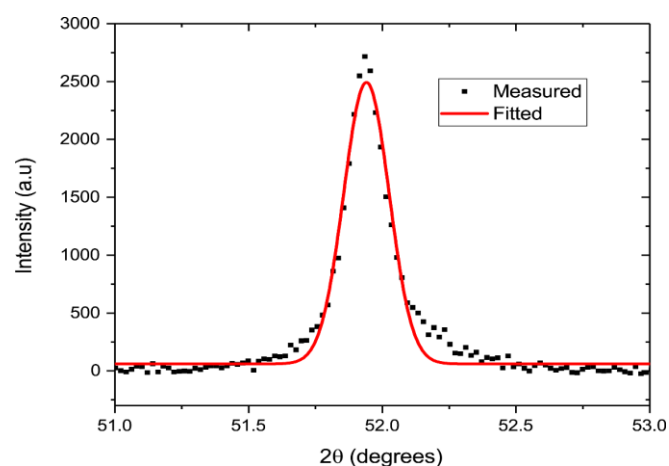


Figure 2 – Diffraction broadening of the TiO₂ film at 2 θ angle of 51.94

A graph of intensity against angle 2θ for the entire spectrum was drawn and all the seven peaks identified.

From Table 1, it was established that the peak at 61.99° , which had a plane orientation of (204),

had the highest FWHM value of 0.007198 radians. This peak is useful in the determination of the morphology index.

Table 1 – Particle size and the d-spacing for the TiO_2 film

Plane	$2\theta(o)$	$\text{Cos } \theta$	$\text{Sin } \theta$	FWHM ($^\circ$)	FWHM (Radian)	$\beta\text{Cos } \theta$	Size (nm)	d-spacing (nm)
(101)	25.83	0.9747	0.2235	0.117	0.002042	0.001990	72.7299	3.4451
(103)	38.24	0.9448	0.3275	0.230	0.004014	0.003793	38.1670	2.3508
(004)	48.53	0.9116	0.4109	0.170	0.002967	0.002705	53.5170	1.8737
(211)	51.94	0.8990	0.4379	0.206	0.003595	0.003232	44.7850	1.7584
(105)	54.37	0.8895	0.4568	0.147	0.002566	0.002282	63.4294	1.6854
(200)	55.54	0.8848	0.4659	0.133	0.002321	0.002054	70.4792	1.6526
(204)	61.99	0.8572	0.5149	0.409	0.007138	0.006119	23.6569	1.4952

Specific Surface Area of TiO_2 compact layer. The specific surface area values were calculated and tabulated in Table 2. Moreover, the surface area to volume ratio was also calculated. Table 2 shows that TiO_2 compact layer had a high surface

area. High surface area was desired because it facilitates the interaction between TiO_2 and the interacting media, like the dye to be used, which primarily happens on the surface or at the interface between the TiO_2 and the dye.

Table 2 – Calculation of SSA of TiO_2 compact layer

Size (nm)	Surface area (nm^2)	Volume (nm^3)	SA to Volume Ratio (nm^{-1})	Specific Surface Area (m^2g^{-1})
72.7299	16,617.9	201,436.5	0.0825	21.8246
38.1670	4,576.411	29,111.28	0.1572	41.5884
53.5170	8,997.749	80,255.47	0.1121	29.6598
44.7850	6,301.092	47,032.44	0.1340	35.4427
63.4294	12,639.52	133,619.4	0.0946	25.0247
70.4792	15,605.37	183,309.5	0.0851	22.5215
23.6569	1,758.203	6,932.298	0.2536	67.0965

From Table 2, the graph of surface area to volume ratio against the particle size of the TiO_2 compact layer was drawn. Figure 3 revealed that surface area to volume ratio and the particle size are inversely related meaning that as the particle size gets smaller, more surface becomes exposed and therefore the surface area increases. Negative gradient also meant that particle has pores which are a useful aspect in terms of dye adsorption into the TiO_2 structure [9].

Morphology Index and dislocation density. As seen from Table 2, the morphology index values of TiO_2 films ranged between 0.5 and 0.78.

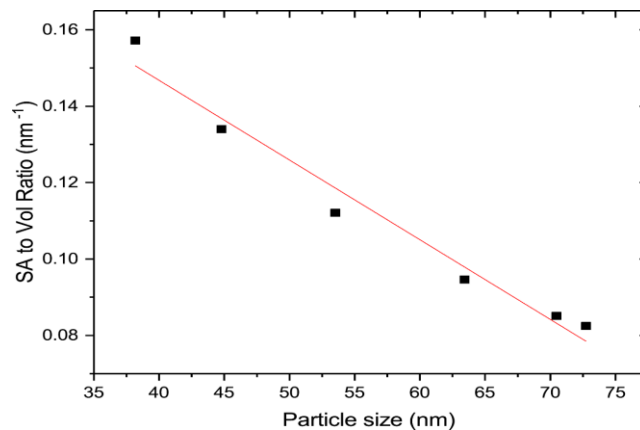


Figure 3 – Graph of surface area to volume ratio against size of particles

Figure 4 shows a linear fitting of the morphology index of TiO₂ compact layer against the particle size. It was observed that MI varies directly as the particle size but with small deviations which confirmed the homogeneity and fineness of the prepared nanoparticles.

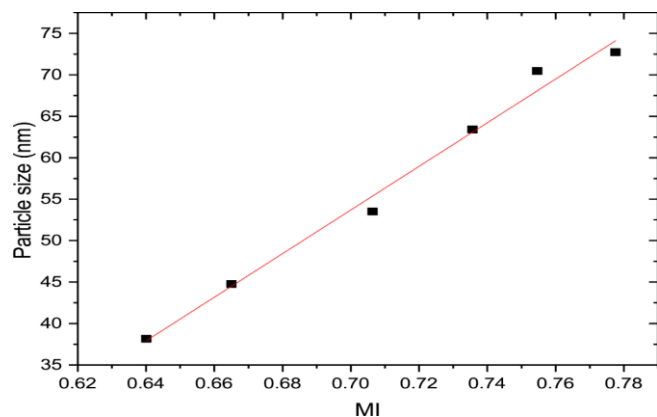


Figure 4 – A linear fitting of TiO₂ particle size against Morphology index

Figure 5 reveals that there exists an inverse relationship between the morphology index and the specific surface area. Just as for the case of the morphology index against the particle size, there

were small deviations between the fitted graph and the experimental points which was an indication that the prepared TiO₂ compact layer had a good uniformity and fineness.

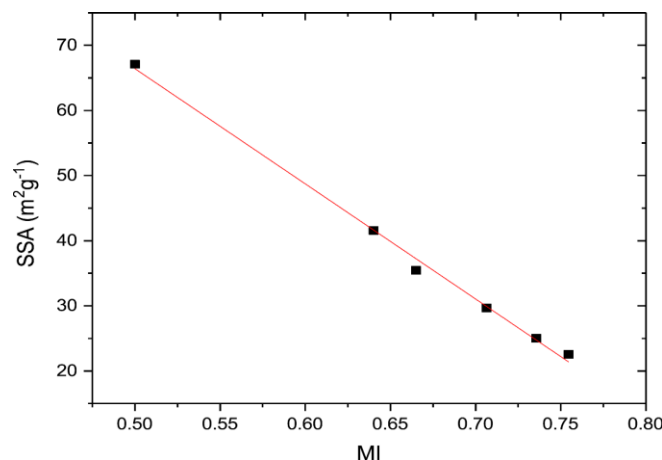


Figure 5 – Linear fitting of SSA against MI of TiO₂ nanoparticles

The results of the dislocation density were tabulated in Table 3.

Table 3 – Dislocation density and Morphology index

FWHM (Radians)	Size (nm)	Surface Area (nm ²)	Volume (nm ³)	Morphology Index	Dislocation Density (m ⁻²)
0.002042	72.7299	16,617.9	201,436.5	0.77756	1.890×10 ¹⁴
0.004014	38.1670	4,576.41	29,111.28	0.64005	6.865×10 ¹⁴
0.002967	53.5170	8,997.75	80,255.47	0.70638	3.492×10 ¹⁴
0.003595	44.7850	6,301.09	47,032.44	0.66503	4.986×10 ¹⁴
0.002566	63.4294	12,639.52	133,619.4	0.73560	2.486×10 ¹⁴
0.002321	70.4792	15,605.37	183,309.5	0.75460	2.013×10 ¹⁴
0.007138	23.6569	1,758.20	6,932.298	0.49999	1.787×10 ¹⁴

Table 3 shows that TiO₂ compact layer had very high dislocation density in the orders of × 10¹⁴ meaning that this film had a good hardness since a large dislocation density means a larger hardness of the material. This was attributed to sintering of the sample.

Figure 6 shows a linear fitting of dislocation density against the particle sizes.

From figure 6, it was observed that dislocation density and the grain size relate inversely. It implies that the prepared TiO₂ compact layer had more strength and hardness than their bulk (TiO₂) counterpart [8].

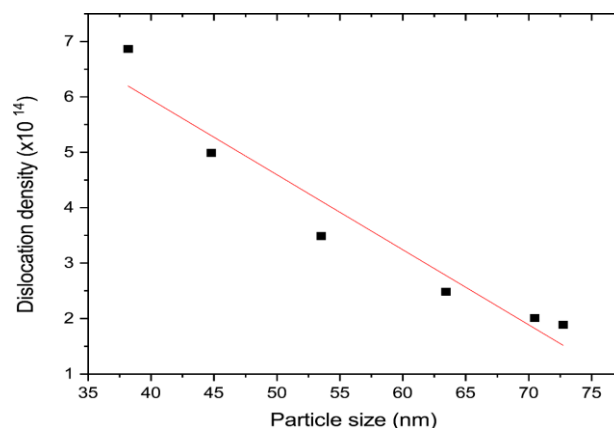


Figure 6 – Dislocation density against the TiO₂ grain sizes

Moreover, there were small deviations between the fitted graph and the experimental points which was an indication that the prepared TiO₂ compact layer had a good film uniformity and fineness of the TiO₂ grains.

Raman spectroscopy

Figure 7 shows Raman spectra of screen printed TiO₂ thin films.

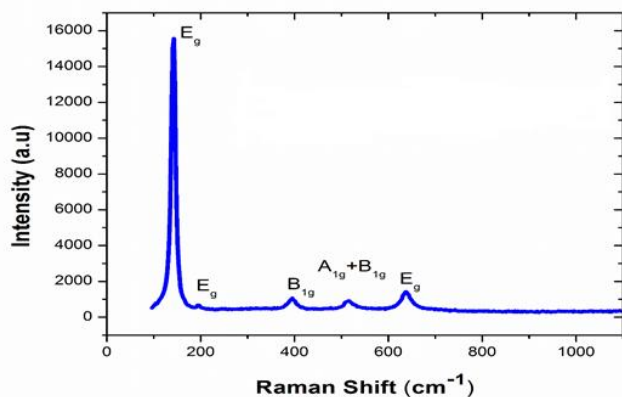


Figure 7 – Plot for the Raman spectra of screen printed TiO₂ thin films

From this figure, the Raman peaks were assigned as E_g , E_g , B_{1g} , $A_{1g} + B_{1g}$ and E_g modes of anatase phase. The first E_g peak was found at 142 cm⁻¹ while the other Raman peaks were found at 195 cm⁻¹, 395 cm⁻¹, 517 cm⁻¹ and 639 cm⁻¹ respectively. These peaks agreed closely to peaks obtained in earlier studies [10] where peaks of 143 cm⁻¹, 197 cm⁻¹, 397 cm⁻¹, 516 cm⁻¹ and 637 cm⁻¹ were reported.

The appearance of an intense peak at 142 cm⁻¹ mode meant that there was a certain degree of long-range order possessed by the TiO₂ nanocrystals [10]. It was the strongest peak and it was attributed to arise from the external vibration of the anatase structure. This peak was also broadened which was attributed to either phonon confinement effect or the surface pressure that is present in materials having sizes of nanometer scale [10].

Hall Effect studies of TiO₂ compact layer

Hall voltage value of 3.62 V was obtained for the TiO₂ compact layer thin film. It was established that this value was positive indicating that the film had a net positive carrier concentration. In TiO₂, the holes served as the majority charge car-

riers in the films and this phenomenon was attributed to donor-type defects like the titanium (cation) interstitials and the oxygen vacancies [11]. TiO₂ has titanium vacancies in its structure and therefore its thin films has p-type properties [12]. However, bulk TiO₂ is an n-type semiconductor.

The TiO₂ film had a Hall coefficient of 0.5 cm³/C. The thickness of the screen printed TiO₂ compact layer thin film was taken to be 116 nm. The Hall coefficient value for TiO₂ thin film agreed very closely with literature [13] where a value of 0.4.998 cm³/C was obtained to be the Hall coefficient of anatase TiO₂ thin film.

By using Four-point probe system interfaced to a computer with Lab-view software and coupled with Keithley 2400 series source meter, the sheet resistance of the screen printed TiO₂ nanoparticle thin films was obtained to be 6.052 × 10⁴ Ω/sq. This sheet resistance translated into resistivity value of 7.02 × 10⁻³ Ω cm which was in agreement with the values reported in literature [14]. From this value of resistivity, the conductivity of the TiO₂ thin film was 1.414 × 10² S/m and therefore the Hall mobility for TiO₂ film was found to be 7.122 × 10¹ cm²/Vs. This Hall mobility for TiO₂ compact layer was considered good and it greatly shows that the TiO₂ films had high crystalline structure.

The final parameter to be calculated for the TiO₂ compact layer thin film was the density of charge carriers. The density of charge carriers in the TiO₂ compact layer was 1.25 × 10¹⁹ cm⁻³. Table 4 summarizes all the parameters studied under Hall Effect.

Table 4 – Summary of Hall Effect parameters of TiO₂ compact layer

Thickness (nm)	Sheet resistance (Ω/sq)	Resistivity (Ω cm)	R_H (cm ³ /C)	n_H (cm ⁻³)	μ_H (cm ² /Vs)
116	6.052 × 10 ⁴	7.02 × 10 ⁻³	0.5	1.25 × 10 ¹⁹	7.122 × 10 ¹

SEM analysis. Figure 8 shows the micrograph of TiO₂ compact layer. The film was relatively smooth because of the slight movement of the glass substrate during the spray pyrolysis deposition process, which was caused by the pressure of the spray. It was also noted that the TiO₂ compact layer coated fully the FTO glass which was desirable in the fabrication of high efficient dye-sensitized solar cell.

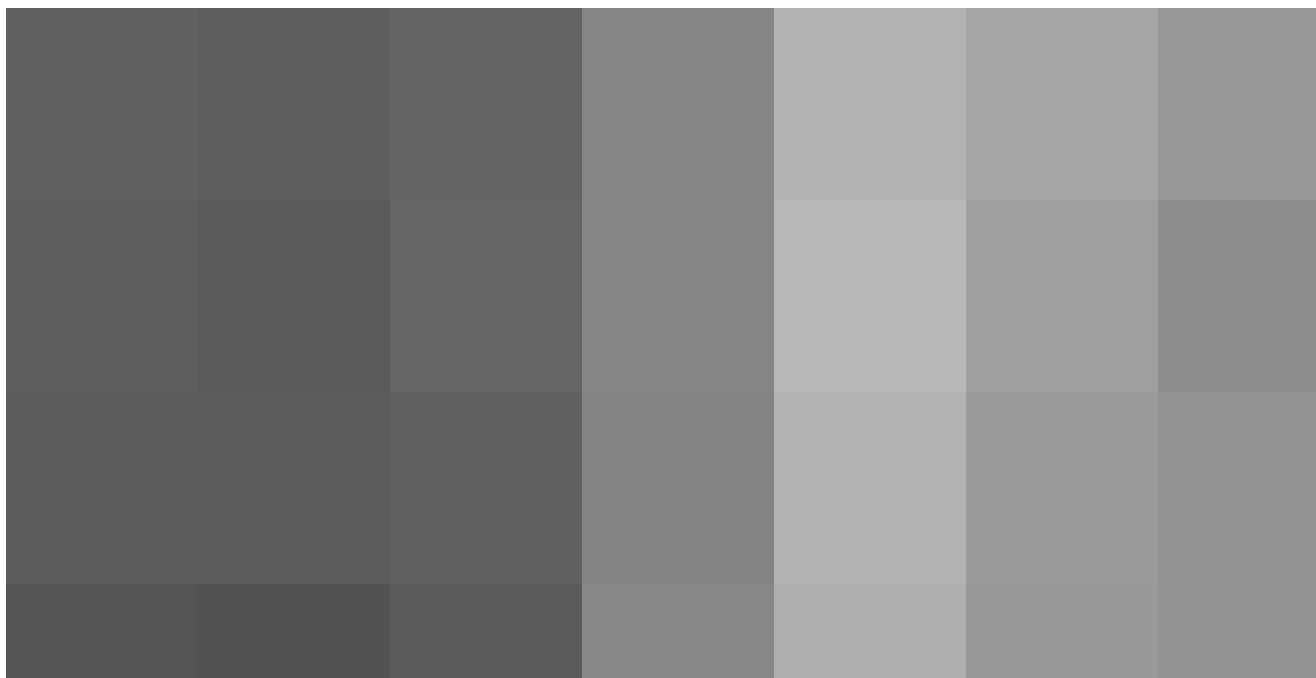


Figure 8 – SEM micrograph of titanium dioxide compact layer

CONCLUSION

TiO₂ compact layer was successfully deposited onto FTO glass substrate using spray pyrolysis techniques. X-ray Diffraction studies revealed that TiO₂ compact layer had tetragonal crystal-line structure with cell parameters $a = 3.7710 \text{ \AA}$ and $c = 9.4300 \text{ \AA}$. Raman spectroscopy showed that TiO₂ compact layer had an intense peak at 142 cm^{-1} mode meaning that there was a certain degree of long-range order possessed by the TiO₂ nano-crystals present in the compact layer. Hall Effect studies revealed that TiO₂ compact layer has high density of charge carriers' value of $1.25 \times 10^{19} \text{ cm}^{-3}$. From these studies, it was concluded that TiO₂ compact layer can be used as a

blocking layer in high performing dye-sensitized solar cells.

ACKNOWLEDGEMENTS

The authors wish to acknowledge Botswana Institute for Technology Research and Innovation for the technical support during the SEM measurements of the samples and Physics department, University of Free State, South Africa for XRD measurements. In addition, this work was supported by the African Development Bank which provided the corresponding author with a scholarship which enabled these studies to be conducted.

REFERENCES

1. Panchal, H., Shah, K. & Padharia, M., (2015). *Dye Sensitized Solar Cells - An Alternative to Silicon Based Photovoltaic Technology*. Retrieved from <https://bit.ly/2NeLy3H>
2. Lewis, N. S., & Nocera, D. G. (2006). Powering the planet: Chemical challenges in solar energy utilization. *Proceedings of the National Academy of Sciences*, *103*(43), 15729–15735. doi: [10.1073/pnas.0603395103](https://doi.org/10.1073/pnas.0603395103)
3. Omata, K., Kuwahara, S., Katayama, K., Qing, S., Toyoda, T., Lee, K.-M., & Wu, C.-G. (2015). The cause for the low efficiency of dye sensitized solar cells with a combination of ruthenium dyes and cobalt redox. *Physical Chemistry Chemical Physics*, *17*(15), 10170–10175. doi: [10.1039/c4cp05981f](https://doi.org/10.1039/c4cp05981f)
4. Sengupta, D., Das, P., Mondal, B., & Mukherjee, K. (2016). Effects of doping, morphology and film-thickness of photo-anode materials for dye sensitized solar cell application – A review. *Renewable and Sustainable Energy Reviews*, *60*, 356–376. doi: [10.1016/j.rser.2016.01.104](https://doi.org/10.1016/j.rser.2016.01.104)

5. Kaur, R., Kim, K.-H., Paul, A. K., & Deep, A. (2016). Recent advances in the photovoltaic applications of coordination polymers and metal organic frameworks. *Journal of Materials Chemistry A*, 4(11), 3991–4002. doi: [10.1039/c5ta09668e](https://doi.org/10.1039/c5ta09668e)
6. Antić, Ž., Krsmanović, R. M., Nikolić, M. G., Marinović-Cincović, M., Mitrić, M., Polizzi, S., & Dramićanin, M. D. (2012). Multisite luminescence of rare earth doped TiO₂ anatase nanoparticles. *Materials Chemistry and Physics*, 135(2-3), 1064–1069. doi: [10.1016/j.matchemphys.2012.06.016](https://doi.org/10.1016/j.matchemphys.2012.06.016)
7. Weirich, T. ., Winterer, M., Seifried, S., Hahn, H., & Fuess, H. (2000). Rietveld analysis of electron powder diffraction data from nanocrystalline anatase, TiO₂. *Ultramicroscopy*, 81(3-4), 263–270. doi: [10.1016/s0304-3991\(99\)00189-8](https://doi.org/10.1016/s0304-3991(99)00189-8)
8. Thirugnanasambandan, T., & Marimuthu, A. (2013). *Titanium dioxide (TiO₂) Nanoparticles - XRD Analyses – An Insight*. Retrieved from https://www.researchgate.net/publication/244990066_Titanium_dioxide_TiO2_Nanoparticles_XRD_Analyses_An_Insight
9. Wolfrom, R. (2012). *Specifics on surface area*. Retrieved from https://www.particletechlabs.com/images/articles/specifics_on_surface_area.pdf
10. Gupta, S. K., Desai, R., Jha, P. K., Sahoo, S., & Kirin, D. (2009, September 15). Titanium dioxide synthesized using titanium chloride: size effect study using Raman spectroscopy and photoluminescence. *Journal of Raman Spectroscopy*. doi: [10.1002/jrs.2427](https://doi.org/10.1002/jrs.2427)
11. Nguu, J., Aduda, B., Nyongesa, F., Musembi, R., Njogu, S., & Mwathe, P. (2015). [Electrical Characterization of Nano-TiO₂/Nb₂O₅ Composite Thin Films Deposited Using Electrophoretic Deposition Technique](#). *International Journal of Innovative Research in Advanced Engineering*, 2, 192–198.
12. Nowotny, M. K., Sheppard, L. R., Bak, T., & Nowotny, J. (2008). Defect Chemistry of Titanium Dioxide. Application of Defect Engineering in Processing of TiO₂-Based Photocatalysts. *The Journal of Physical Chemistry C*, 112(14), 5275–5300. doi: [10.1021/jp077275m](https://doi.org/10.1021/jp077275m)
13. Tang, H., Levy, F. (1995). *Electronic properties of anatase TiO₂ investigated by electrical and optical measurements on single crystals and thin films*. Retrieved from <https://infoscience.epfl.ch/record/31789>
14. Daniyan, A. A., Umoru, L. E., Fasasi, A. Y., Borode, J. O., Oluwasegun, K. M., & Olusunle, S. O. O. (2014). Electrical Properties of Nano-TiO₂ Thin Film Using Spin Coating Method. *Journal of Minerals and Materials Characterization and Engineering*, 02(01), 15–20. doi: [10.4236/jmmce.2014.21003](https://doi.org/10.4236/jmmce.2014.21003)